ADVANCED SUSTAINABLE SYSTEMS
www.advsustainsys.com

Role of Potassium in Electrocatalytic Water Oxidation Investigated in a Volume-Active Cobalt Material at Neutral pH

*Si Liu, Shima Farhoosh, Paul Beyer, Stefan Mebs, Ivelina Zaharieva, Michael Haumann, and Holger Dau**

The oxygen evolution reaction (OER) is crucial in systems for sustainable production of hydrogen and other fuels. Catalytic OER materials often undergo potential-induced redox transitions localized at metal sites. For volume-active catalyst-materials, these are necessarily coupled to charge-compensating relocation of ions entering or leaving the material, which is insufficiently understood. The binding mode and mechanistic role of redox-inert ions for a cobalt-based oxyhydroxide material (CoCat) when operated at neutral pH in potassium-phosphate (KPi) electrolyte are investigated by i) determination of K:Co and P:Co stoichiometries for various KPi-concentrations and electrode potentials, ii) operando X-ray spectroscopy at the potassium and cobalt K-edges, and iii) novel time-resolved X-ray experiments facilitating comparison of K-release and Co-oxidation kinetics. Potassium likely binds non-specifically within water layers interfacing Co-oxyhydoxide fragments involving potassium–phosphate ion pairs. The potassium-release kinetics are potential-independent with a fast-phase time-constant of about 5 s and thus clearly slower than the potential-induced Co oxidation of about 300 ms. It is concluded that the charge-compensating ion flow is realized neither by potassium nor by phosphate ions, but by protons. The results reported here are likely relevant also for a broader class of volume-active OER catalyst materials and for the amorphized near-surface regions of microcrystalline materials.

1. Introduction

The water oxidation reaction (or oxygen evolution reaction, OER) is a pivotal process in producing non-fossil carbon-free (hydrogen gas, H_2) or carbon-based (e.g., methanol) fuels as sustainable energy resources of the future. Numerous catalyst materials have been extensively investigated for improving electrocatalytic OER protocols.[1–6] Naturally, the focus is often on the properties of the transition metals (for example Mn, Fe, Co, Ni, Ir, and Ru) that are present in the catalyst material, inter alia because they are often redox-active, meaning that their oxidation state varies reversibly in response to an applied electric potential.[7–11] Also the role in OER of redox-inert cations present in the electrolyte and/or within the catalyst material has been investigated,[12–21] but their function is still insufficiently understood. A more complete understanding is desirable to promote rationale, knowledge-guided development of superior OER catalyst materials.

Here, we investigate the role of potassium ions in a cobalt-based, volume-active[8] catalyst material which contains K^+ as well as phosphate ions.[22] This oxyhydroxide material, in the following denoted as CoCat, has been especially well investigated[23–30] and can serve as a model system in mechanistic investigations on water oxidation (OER) by non-noble metal materials in the environmentally friendly neutral-pH regime.[7,31–33] Central open questions regarding the role of potassium ions are:

(1) What is the structural role of K^+ ions bound within the Co-Cat material? In our earlier Co K-edge extended X-ray absorption fine structure (EXAFS) analysis, the presence of Co(μ-O)K motifs with a Co–K distance of ≈3.8 Å was proposed.[28] Subsequently, Kanan et al. compared the EXAFS spectra of potassium-phosphate (KPi-) CoCat and sodium-phosphate (NaPi-) CoCat and found no structural difference.[23] Ex situ X-ray absorption spectroscopy (XAS) at the potassium K-edge suggested that ≈10% of K^+ ions might be constituents of (distorted) $KCo_3(\mu\text{-}O)_4$ cubane structures.[13] The question remains whether potassium ions can be part of specific K-Co coordination motifs, that is, in cubane structures similar to those suggested for calcium (Ca^{2+}) ions in Ca-containing Mn

S. Liu, S. Farhoosh, P. Beyer, S. Mebs, I. Zaharieva, M. Haumann, H. Dau
Department of Physics
Freie Universität Berlin
Arnimallee 14, 14167 Berlin, Germany
E-mail: holger.dau@fu-berlin.de

The ORCID identification number(s) for the author(s) of this article can be found under https://doi.org/10.1002/adsu.202300008

DOI: 10.1002/adsu.202300008

oxides,[34–37] with analogies to the biological (Mn_4Ca) OER catalyst of oxygenic photosynthesis.[38–40]

(2) Do K^+ ions facilitate charge compensation in the redox transitions of the catalyst material? The potential-dependent redox transitions of the CoCat bulk material ($Co^{2+} \leftrightarrow Co^{3+} \leftrightarrow Co^{4+}$) involve proton-coupled electron transfer and likely charge-compensation by proton release (for Co oxidation) or uptake (for Co reduction).[5,7,31] However, whether K^+ ions or other redox-inactive cations can also participate in the charge compensation process is insufficiently understood. A role of K^+ uptake and release for alkaline OER in KOH electrolyte indeed has been suggested recently. Grimaud et al. reported K^+ insertion into layered iridium oxides during OER, with the insertion process incurring a phase transformation of oxidized α-Li_1IrO_3 coupled with Ir reduction and K^+ ions likely participating in the overall charge balance process.[41] For NiFe and CoFe oxyhydroxides, Strasser and coworkers reported α to γ phase conversions and contraction of lattice spacing in the OER catalytic regime,[42] as induced by Co/Ni oxidation and associated with intercalation of K^+ ions.

Here, we provide insights by addressing experimentally 1) the structural and 2) the charge-compensating role of K^+ ions for the Co-based catalyst material which may serve as a model system for OER at neutral pH in general. Progress comes from monitoring the response of CoCat electrocatalytic films to electrolyte variations and changes in electrical potential by quantitative elemental analysis, experimentally challenging ex situ and in situ (operando) XAS at the potassium K-edge, and novel time-resolved X-ray experiments.

2. Results and Discussion

2.1. Elemental Analysis after Variation of Electrolyte and Electrode Potential

Potassium as well as phosphate have been verified to be internal constituents of CoCat at an approximate Co:P:K ratio of 2–3:1:1, for catalyst films electrodeposited in 100 mM potassium phosphate (at pH 7).[22] The question remained whether and how the potassium content of the catalyst film changes during operation i) in electrolytes with varying K^+ concentrations and ii) in response to changes of the electrode potential. Therefore, elemental analysis was carried out for CoCat films after operation at different KPi concentrations (1.6, 25, or 100 mM) or electrode potentials (1.0 or 1.3 V vs NHE); the results are summarized in **Figure 1**. Noteworthy, the CoCat undergoes the same oxidation state and structural changes in response to the electrode potential at all three KPi electrolyte concentrations.[32]

We determined molar ratios of ≈0.3 for K:Co and ≈0.4 for P:Co and thus of ≈1.3 for P:K for films electrodeposited at 1.05 V_{NHE} and operated at 1.3 V_{NHE} (both in 100 mM KPi, pH 7). These figures are close to previously reported values for CoCat films electrodeposited at 1.29 V_{NHE} in 100 mM KPi, thus verifying the reproducibility of the molar ratios of the main CoCat ingredients as resulting from different electrodeposition and elemental quantification protocols.[22] Figure 1 furthermore reveals:

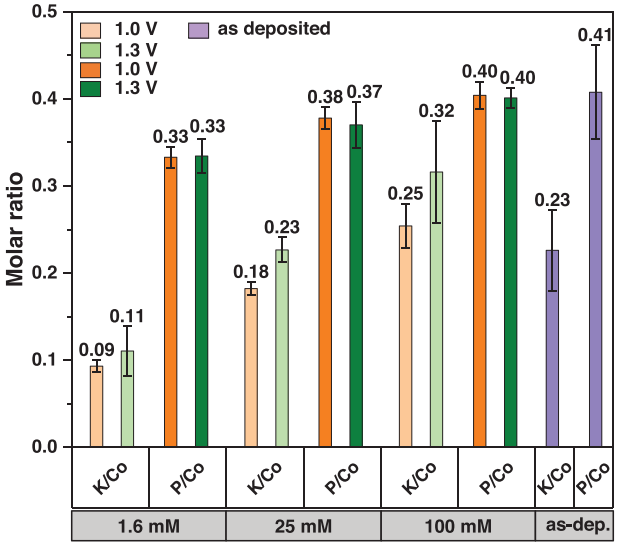

Figure 1. Molar ratio of potassium, phosphorus, and cobalt for CoCat films after operation at two electrode potentials (1.0 or 1.3 V vs NHE, pH 7) and in various electrolyte concentrations of potassium phosphate (KPi). Each film was operated at the indicated electrode potential for 15 min. The molar ratios for CoCat directly after electrodeposition in 100 mM KPi are labeled by "as deposited" or "as-dep." The K/Co ratios resulted from three experiments on three CoCat films; for each CoCat film, minimally three quantifications of the Co and K^+ contents were conducted; error bars show standard deviations. For further details, see Figures S1 and S2 and Tables S1–S3, Supporting Information. The molar ratios of P and Co were calculated from data reported by us elsewhere.[32] Here the molar K/Co ratios were determined for CoCat films deposited on a platinum sheet whereas the P/Co quantification refers to films deposited on indium tin oxide (ITO); there are no indications that the substrate electrode material affects the elemental composition of the comparably thick CoCat films (≈140 nm[8,43]).

(1) The K:Co stoichiometry is not a constant but depends strongly on the K^+ concentration during electrocatalytic operation; by a factor of ≈3 smaller K:Co ratio was found for CoCat operation in 1.6 versus 100 mM KPi. In contrast, the P:Co ratio showed much smaller variations (≤20%) for the same large KPi concentration change. This suggests comparably weak binding of the majority of potassium ions within the CoCat material, which is further supported by the complete and rather fast potassium–sodium exchange reported further below (Figure 5B,C).

(2) Both the P:Co and the K:Co molar ratios are essentially potential-independent, excluding that these ions contribute significantly to charge compensation in response to the massive potential-induced valence changes of the Co ions, as explicated in the following.

As we already reported,[32] the phosphate content of CoCat films is fully potential-independent ruling out that phosphate uptake facilitates charge compensation upon oxidation of Co ions. For the K:Co molar ratio, we observe a trend toward a slightly increased K^+ content in response to operation at catalytic versus pre-catalytic potential. However, this trend is not only of debatable statistical significance, but also the observation of increased K^+ content for Co oxidation (positive charging of Co ions) rather

would suggest a minor K^+ uptake than charge compensation by K^+ release.

The extent of the contradiction between the data in Figure 1 and charge balancing by uptake/release of phosphate or K^+ ions is particularly evident when comparing the fraction of Co ions that undergo valence changes. The increase in electrode potential from 1.0 V_{NHE} to 1.3 V_{NHE} is associated with an increase in the mean Co oxidation state from about 2.75 to 3.13,[7,32] which corresponds to 0.38 oxidizing equivalents (positive charges) per Co ion. Consequently, for the CoCat operated in 100 mM KPi electrolyte, the potential increase from 1.0 to 1.3 V_{NHE} would require release of all K^+ ions to compensate for the charging of the material by Co oxidation, whereas not any release of K^+ ions was detected. For operation at 1.6 mM KPi, even the release of all K^+ ions could not provide efficient charge compensation because the total amount of K^+ ions is too low. Similarly, also the potential-independent phosphate content excludes charge-compensation by phosphate uptake or release. Therefore, we can safely conclude that neither K^+ ions nor phosphate ions facilitate charge compensation in the redox transitions of the CoCat material.

We note that the amount of Co ions undergoing potential-dependent valence changes was determined by X-ray spectroscopy with X-ray energies of 7–8 keV,[7,32] where the X-ray penetration depth (hundreds of micrometer) vastly exceeds the CoCat film thickness (≈700 nm). Therefore, the above estimate of oxidation of 38% of the Co ions undergoing valence changes does not rely on bulk-uniform redox properties of the CoCat material. Nonetheless, most likely the oxidation-state changes indeed proceed homogeneously throughout the CoCat bulk material.[8]

The bulk-uniform redox chemistry is a central concept in the discussion of CoCat material properties that has been addressed previously[7,8] and is also relevant here when discussing charge-compensating ion movements. The bulk-uniform Co valence changes[7,8] suggest that the binding of redox-inactive ions and charge compensation by ion uptake or release is also uniform throughout the catalyst material. In a small near-surface region, mobile CoCat-external electrolyte ions could provide charge compensation, describable as electric (ionic) double-layer formation. However, both catalytic performance and our experimental analyses are clearly dominated by the CoCat bulk material.[43] In summary, it is adequate to discuss herein the K^+ binding motifs and charge-compensating ion movements assuming a bulk-uniform behavior. Irrespective of complete bulk-uniformity, the data of Figure 1 excludes charge-compensation by neither potassium nor phosphate ions.

2.2. Potassium Coordination from X-Ray Absorption Spectroscopy

2.2.1. Comparison of X-Ray Absorption Near-Edge Structure Spectra

The CoCat material belongs to the family of amorphous layered oxyhydroxides of the MO_2 type (M = Mn, Co, Ni, Ru, and Ir), but is distinguished by especially small MO_2 fragments possibly comprising less than 20 Co ions.[7,23,28,29,44,45] The layered-oxide fragments of CoCat are likely not directly stacked, but separated by water molecules and ions, namely potassium and phosphate.[7,23,28,29,44,45] The CoCat thus resembles the well-known birnessite structures of Mn oxides or other layered oxides, for which intercalated cations, typically alkali metals or alkaline earth metals, are widely found.[41,46–50] The K^+–M distance is typically around 3.0–3.5 Å.[13,47,51,52] Since the CoCat material is highly amorphous and thus does not diffract, XAS is the method of choice for structural investigation of such catalyst films, which are volume-active regarding oxidation-state dynamics and OER catalysis.[8] Whereas pair distribution function analysis on CoCat has been used to study domain size and structural features, it does not provide an element-specific focus,[53–55] in contrast to our present EXAFS analysis revealing the K^+ binding motifs. XAS at the Co K-edge has been repeatedly applied to CoCat material for assessment of Co oxidation states (electronic structure), via analysis of the X-ray absorption near-edge structure (XANES), and for insight in the atomic structure, via analysis of the EXAFS.[7,23,28,31,32,44] Here, we provide complementary structural information by XANES and EXAFS analyses at the potassium K-edge, which is experimentally challenging and has been applied before only once to the CoCat material (to our knowledge).[13]

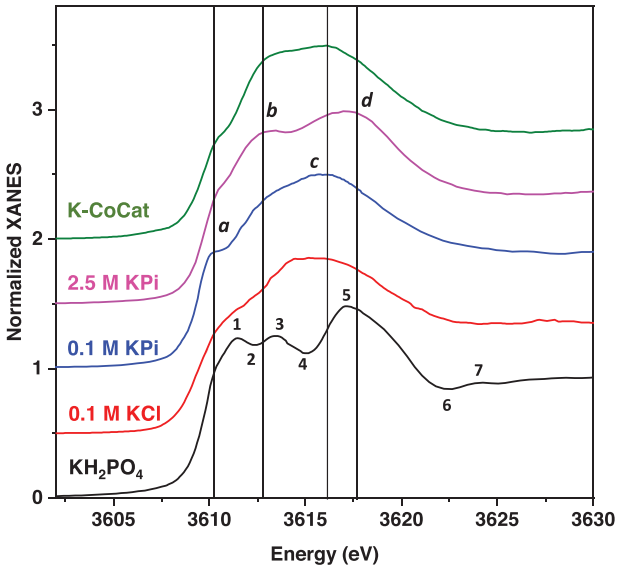

Figure 2. Comparison of potassium K-edge XANES spectra for dry CoCat film (K-CoCat) and potassium reference compounds. XANES spectra were collected for CoCat films, microcrystalline KH_2PO_4 powder, and aqueous solutions of cobalt phosphate (KPi) at 0.1 M or 2.5 M (pH 7), and an aqueous KCl solution at 0.1 M. The 2.5 M KPi spectrum was corrected for self-absorption (Figures S6 and S7, Supporting Information). For further details of the measurement conditions (temperature), see section 1.3 and Figure S6, Supporting Information. Spectra are stacked for clarity. Prominent features are marked by lower-case letters and for KH_2PO_4 by numbers.

Visual comparison of the K-edge spectra in **Figure 2** reveals overall similar, but not identical spectra of CoCat and K^+ ions in solution (0.1 M KCl, 0.1 M KPi, and 2.5 M KPi), suggesting a K^+ coordination environment in the CoCat that is quite similar to that of hydrated K^+ ions, but differs in specific features. The 2.5 M KPi spectrum is expected to differ from the 0.1 M KPi spectrum due to the presence of an increased number of potassium–phosphate ion pair interactions at high KPi concentrations. We assign features *b* and *d* to ion pair interaction because these features are

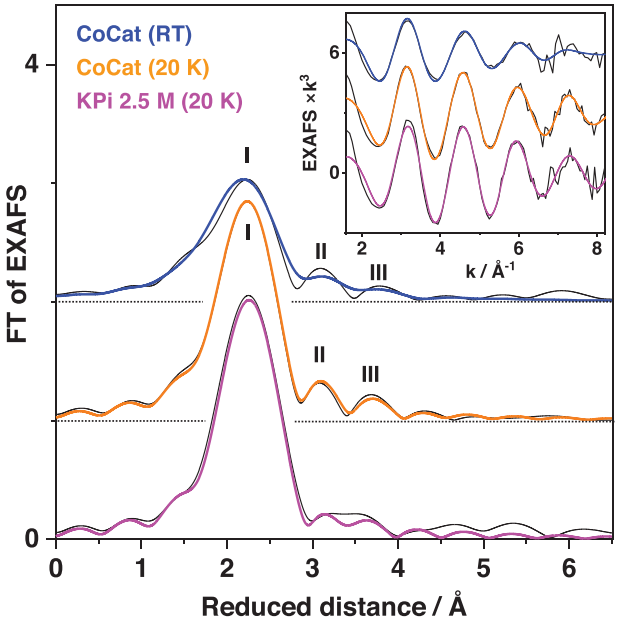

Figure 3. EXAFS analysis of CoCat films and KPi solution. Spectra were collected at 20 K or room temperature (RT). The main panel shows Fourier-transforms (FTs, calculated from 1.6–8.2 $Å^{-1}$) of the EXAFS oscillations in the inset (experimental data, black lines; simulations with parameters in Table 1, colored lines). Spectra are vertically stacked for clarity.

Table 1. EXAFS simulation parameters in Figure 3.

shell	CoCat RT R_f = 12.9%			CoCat 20 K R_f = 4.6%			KPi 20 K R_f = 7.3%		
	N [K^{-1}]	R [Å]	$2\sigma^2$ [$Å^2$]	N [K^{-1}]	R [Å]	$2\sigma^2$ [$Å^2$]	N [K^{-1}]	R [Å]	$2\sigma^2$ [$Å^2$]
K–O	7[a)]	2.74	0.059[b)]	7[a)]	2.76	0.029[b)]	7[a)]	2.76	0.027[b)]
K–P	0.9	3.51	0.059[b)]	0.5	3.45	0.029[b)]	0.4	3.67	0.027[b)]
K–Co	0.8	4.21	0.059[b)]	0.5	4.13	0.029[b)]	/	/	/

[a)] Coordination numbers were set to 7; [b)] The Debye–Waller parameter ($2\sigma 2$) resulted from a joint fit to yield the same value for all coordination shells. The fit error parameter, R_f, was calculated for reduced distances of 1–4 Å.[56]

well resolved in the 2.5 M KPi spectrum and merely absent in the 0.1 M KPi and KCl spectra. Vice versa, the features denoted *a* and *c* are more prominent in 0.1 versus 2.5 M KPi. In the CoCat spectrum, the discernible *b*-feature and the *d*-feature shoulder, as well as the relatively diminished features *a* and *c* suggest that potassium–phosphate ion pair formation, with phosphate ions in the first K^+ coordination sphere, to some extent occurs also in the CoCat. In comparison to micro-crystalline solid KH_2PO_4 (or K_2HPO_4, data not shown), we note the absence of pronounced features typical for crystalline materials (1–6 in Figure 2) in the CoCat XANES spectrum, suggesting that (nano-) crystalline domains of $K_xH_yPO_4$ are not present within the CoCat material.

2.2.2. Analysis of EXAFS Spectra

Selected EXAFS spectra are shown in **Figure 3**; for experimental details, further spectra, and EXAFS simulation parameters see Supporting Information (**Table 1**).

The EXAFS spectra of CoCat collected at 20 K or room temperature (RT) reveal (within noise limits) similarity of the main interatomic interactions, for example, K–O bonds (peak I in the FT-spectrum), which are also detectable in the 2.5 M KPi EXAFS (see Table 1). The EXAFS oscillations in the RT spectrum of CoCat are overall similar to that of the 20 K spectrum, indicating the absence of significant structural changes upon freezing of the material. The clearly more damped EXAFS amplitudes in the RT spectrum are expected due to increased vibrational disorder (increased Debye–Waller factors), which hence are closer to the noise level. This difference motivates our focus on the 20 K spectra. The coordination number (N) of hydrated K^+ is consistent with 6 ± 2 oxygen atoms (from water molecules or O-atoms within CoCat) surrounding the K^+ ion;[57] a coordination number close to 7 seems likely[58,59] (**Figure 4**, motif δ). In our EXAFS simulations, the longer distances relating to peaks II and III in the FT-spectrum are modeled as a K–O–PO_3 motif (peak II, K–P around 3.5 Å, motif γ in Figure 4) and a K–O–Co motif (peak III, K–Co around 4.1 Å, motif β in Figure 4). For both motifs a low coordination number of about 0.5 is well compatible with the experimental data. EXAFS fit-error contour plots reveal parameter correlations and likely coordination number boundaries (Figure S5, Supporting Information). A more precise determination of N_K and N_{Co} cannot be reached from the present data, but values significantly exceeding 0.5 P and 0.5 K distances per Co center seem to be unlikely.

The cubane-type binding of K^+ to a central Co ion of a CoO_2 layer fragment (motif α in Figure 4) predicts an N_{Co} of 3 for the nearest Co ions at around 3.4–3.6 Å and additionally a similarly high N_{Co} for the next-nearest Co ions of the CoO_2 layer fragment at around 4.6 Å. For interconnection of two layers by a K^+ ion, the corresponding coordination numbers could be as high as 6. These figures are so much larger than the experimental value that we can exclude binding of a sizeable fraction of K^+ ions in form of well-ordered $KCo_3(\mu_3\text{-}O)_4$ cubanes. However, highly disordered or loose binding of a sizeable fraction of K^+ ions via a single O-atom to CoO_2 layer fragments (motif β) is compatible with the EXAFS data.

The formation of potassium–phosphate ion pairs (motif γ in Figure 4) is supported by the XANES spectra (as discussed further above) and in line with the EXAFS analysis. The EXAFS analysis leads to values of N_{Co} and N_P around 0.5 which suggests that for six to sevenfold coordination of K^+ to O^-atoms, the majority of coordination partners are likely water molecules present in the space between CoO_2 layer fragments.

2.3. In Situ XAS Detecting K^+ Exchange Kinetics

The CoCat undergoes potential-dependent redox transitions of the amorphous bulk material, with the mean Co oxidation states ranging from about +2.6 at low potentials to about +3.2 at catalytic potentials.[7] For basic physical reasons, the Co oxidation (reduction), within the bulk of the CoCat films of significant thickness, essentially needs to be coupled to stoichiometric charge-compensating ion uptake or release, with ions moving between the CoCat bulk and the electrolyte. By comparison of the K^+ content of the CoCat material equilibrated at various electrolyte concentrations and electrode potentials (Figure 1), we

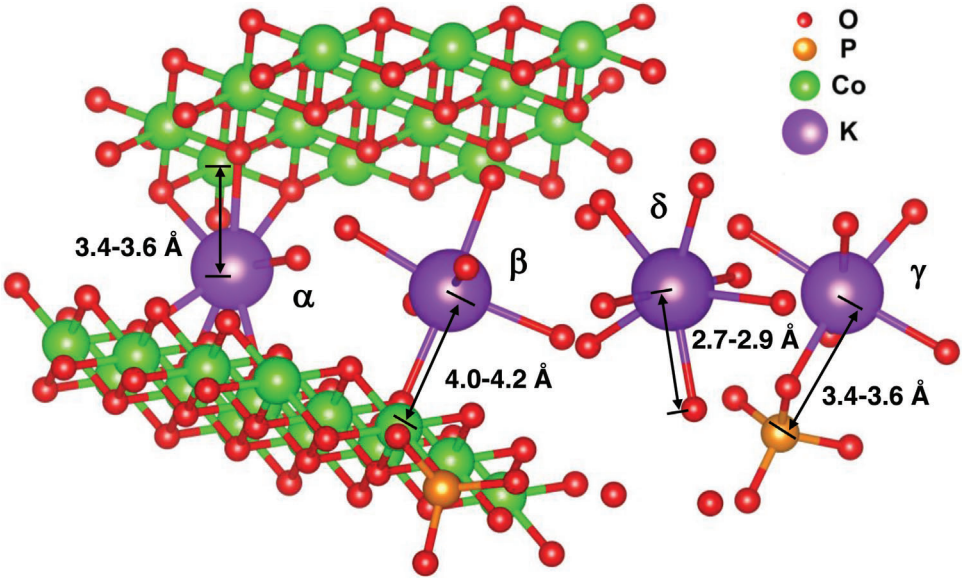

Figure 4. Hypothetical structural motifs of potassium binding in the CoCat material. Two-layer fragments interconnected by binding to the same interlayer K^+ ions are shown. *α*) K^+ bound to three oxygen atoms of a CoO_2 layer fragment forming a $KCo_3(\mu\text{-}O)_4$ cubane motif. *β*) K^+ bound via one oxygen atom to a Co ion of the CoO_2 layer fragment; K^+ binding via an O-atom bridging between Co ions or to a terminal oxygen of a CoO_2 layer fragment is conceivable. *γ*) Ion-pair of K^+ and phosphate ($H_xPO_4^{-(3-x)}$) formed via one bridging oxygen atom. *δ*) Fully hydrated K^+ ion present in the interlayer region of neighboring CoO_2 layers without O-bridging to Co ions. The indicated distances or distance ranges represent estimates that are compatible with the EXAFS data.

showed that neither K^+ nor phosphate ions facilitate charge-compensation in the equilibrated catalyst film, supporting XAS investigations that suggested charge compensation in the $Co^{2+/3+}$ and the $Co^{3+/4+}$ transitions by protonation-state changes of bridging or terminal oxygen ligands of Co ions.[7,31] However, merely based on the results obtained for the fully equilibrated CoCat, the following scenario cannot be excluded:

In an initial response to an increased potential, K^+ ions leave the catalyst material, which may be understood as charging of double-layer capacities at CoCat-intrinsic nanoscopic surfaces. Subsequently, structural changes associated with deprotonation and proton release proceed, which are coupled to K^+ uptake from the electrolyte.

To scrutinize the above scenario, we developed a novel in situ X-ray experiments showing that the K^+ release from the CoCat material is significantly slower than the redox transitions, thereby precluding transient K^+ release preceding the (oxidative) redox transition of the bulk material. The in situ XAS detection mode is illustrated in Figure S3, Supporting Information; for the timing protocol and time courses of K^+ release, see **Figure 5**. Briefly, the X-ray fluorescence far above the potassium K-edge, which is proportional to the detectable amount of potassium in the CoCat film, was monitored in time before and after sudden exposure to a potassium-free electrolyte (NaPi), to follow the release of K^+ from the catalyst, which most likely proceeds in form of a K^+ versus Na^+ exchange.

The concentration of K^+ ions within the CoCat film decreases monotonously after exposure of the K^+-containing CoCat film to NaPi electrolyte (Figure 5B), with an estimated half-time around 5 s. The Co oxidation-state changes can proceed clearly faster, as shown further below, excluding K^+ release as the concomitant charge-compensating ion flow. The K^+ release, which presumably proceeds as a K^+/Na^+ exchange here, represents an essentially complete K^+ depletion, as indicated by the practically negligible amplitude of the final potassium X-ray absorption spectrum (Figure 5C and Figure S12, Supporting Information). This finding indicates that there is no major fraction of K^+ ions that are firmly bound within the CoCat, in line with the above observation of a comparably large change of the K amount upon variation of the KPi concentration (Figure 1). Notably, XAS data at the Co K-edge show that the CoCat film was fully stable (Figures S13 and S14, Supporting Information), indicating that within the time course of the kinetic experiment, K^+ release is not related to any film degradation.

The absence of a significant influence of K^+/Na^+ exchange on the Co K-edge XAS spectra of the CoCat indicates similar structures under both conditions (Figures S13, S14, and S15B, Supporting Information), in agreement with earlier data.[23] Our K-EXAFS data (above) suggested a coordination number of K(–O–)Co distances (N_{Co}) around 0.5, which, when taking the Co:K stoichiometry of 3:1 as it is expected for cubane-type binding into account, would correspond to a coordination number of only about 0.17 (=0.5/3) in the Co-EXAFS. For a coordination number of 0.17 with a likely sizeable Debye–Waller factor (σ), a discernible contribution of a K(–O–)Co distance to the Co K-edge EXAFS spectra is not expected. We conclude that both the K^+ and the Co EXAFS are compatible with only rare occurrence of K(–O–)Co distances.

Noteworthily, application of an electric potential is not required to induce K^+/Na^+ exchange, because similarly fast K^+ release was observed without any applied potential (OCP transient in Figure 5B) or at pre-catalytic (0.65 V_{NHE}) or catalytic (1.35 V_{NHE}) potentials. Visual inspection of the normalized K^+ fluorescence traces in Figure 5B appears to indicate slightly more rapid K^+

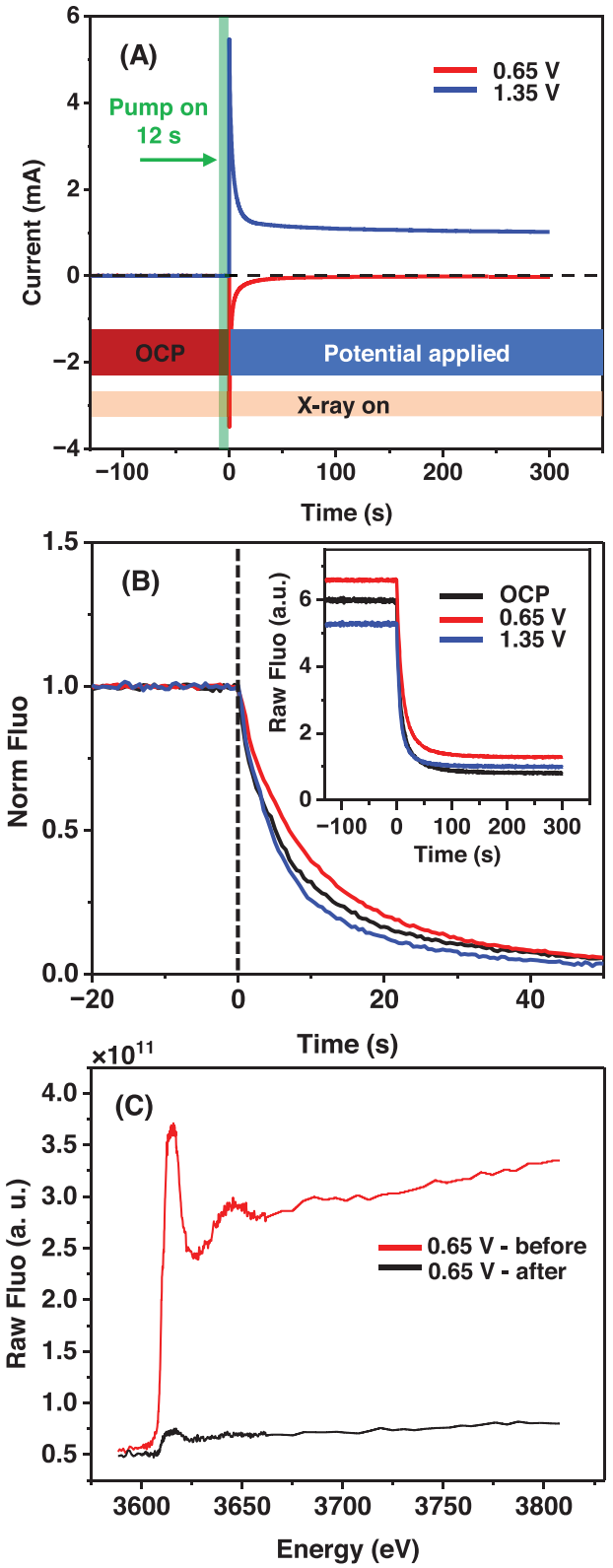

Figure 5. Time-resolved X-ray experiment for tracking K^+ release from CoCat films. A) Experimental protocol and current traces. B) Time course of the potassium K_α-fluorescence for X-ray excitation at 4 keV, reflecting the detectable amount of K^+ within the CoCat film; the inset shows the same data on an expanded time scale, but without signal normalization. C) Potassium K-edge X-ray absorption spectra (non-normalized I_{fluo}/I_0 data) collected on the dry film "before" K^+ release and "after" exposure for 15 min to the continuously stirred NaPi electrolyte, illustrating that most or even all K^+ ions leave the CoCat film when exposed to NaPi (spectra shown here are for CoCat operated at 0.65 V_{NHE}; data for other potentials are shown in Figure S12, Supporting Information). For detection of K^+ release kinetics, dry CoCat films previously electrodeposited in 100 mM KPi were exposed to 100 mM NaPi electrolyte by filling the three-electrode cell using a pump system within 12 s, with more sudden exposure of the X-ray irradiated CoCat areas to the NaPi electrolyte (<2 s). At this point K^+ ions started to leave the catalyst material ($t = 0$ in B), resulting in the decrease of the X-ray fluorescence shown in panel B. Roughly at the same time ($t = 0$ in panel A), either a potential of 0.65 V_{NHE} or of 1.35 V_{NHE} was applied for 10 min, or the open-circuit potential (OCP) condition continued; for complete time traces see Figure S10, Supporting Information. CoCat film thickness corresponding to 100 mC cm^{-2} deposition charge; deposition on graphene sheets; KPi and NaPi at pH 7; and rapid stirring of NaPi electrolyte to remove K^+ ions released from the CoCat film.

release for CoCat films operated at 1.35 V_{NHE} (Co oxidation, positive currents) than at 0.65 V_{NHE} (Co reduction, negative currents), and K^+ release at an intermediate rate without any applied potential (OCP, no Co oxidation-state change). However, potential jumps to further potentials (Figure S9, Supporting Information) and also simulations of K^+-release traces (Figure S10 and Table S4, Supporting Information) do not support a potential-dependence of the K^+ release kinetics; the scatter in the experimental transients may relate merely to limited reproducibility of the NaPi-electrolyte exposure rate. Also another experimental approach, involving a series of short (1 s) potential-steps during the NaPi-exposure period (Figure S11, Supporting Information), does not support an electric-potential dependence of the K^+ release rate. In summary, the role of redox-inert cations inside of CoCat was studied via operando-XAS at the potassium K-edge, revealing comparably weak binding of K^+ in the material and, importantly, the absence of any significant charge compensation role for K^+ ions.

2.4. Time-Resolved XAS Experiment at the Cobalt K-Edge

For CoCat films of similar thicknesses as employed in the K^+ release experiments, we explored the response of the Co oxidation state to applied electrode potentials in time-resolved X-ray absorption experiments. For this, the intensity of the Co K_α-fluorescence at a selected fixed X-ray excitation energy about at half-height of the Co K-edge, which is sensitive to the cobalt oxidation state, was monitored with a time-resolution of 1 ms (**Figure 6**). Simulation analysis permitted determination of the time constants of the cobalt redox transition. The underlying rationale is described in ref. [33] and in the legend of Figure S16, Supporting Information. The potentials were chosen such that a 0.75 → 1.1 V_{NHE} jump induced the $Co^{2+} \rightarrow Co^{3+}$ transition whereas a 1.2 → 1.35 V_{NHE} jump into the catalytic regime induced the $Co^{3+} \rightarrow Co^{4+}$ transition. Notably, both redox transitions do not involve all Co ions of the CoCat material.[7]

For both potential jumps in Figure 6, a fast phase (τ below 400 ms) and a slow phase (τ about 1–4 s) are well resolved. Both phases clearly correspond to Co oxidation, by electron transfer to the working electrode (see current traces in Figure 6A), and

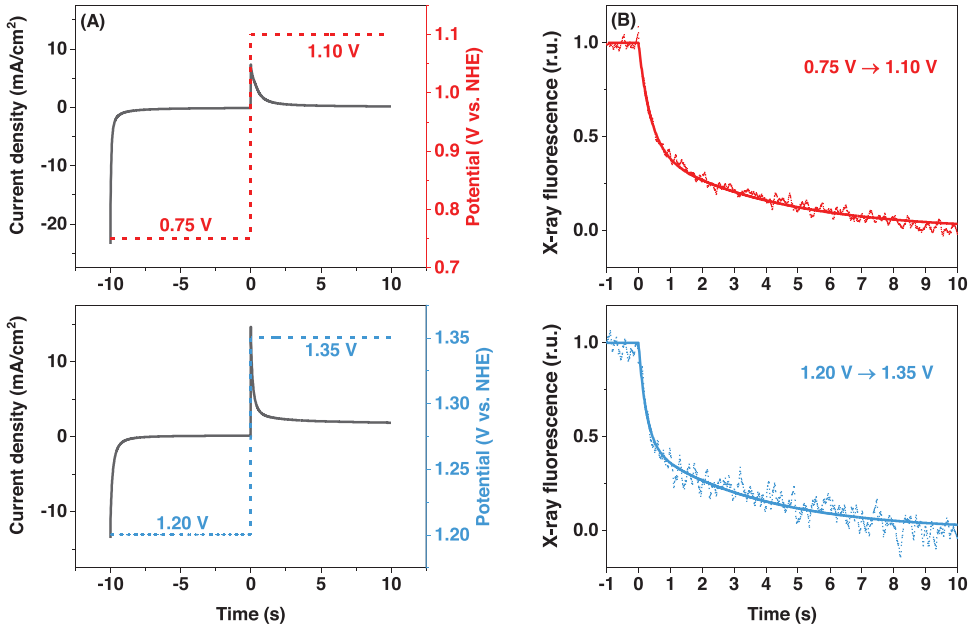

Figure 6. Time-resolved potential-jump operando-XAS on CoCat films at the Co K-edge. A) Working electrode potential and current density for 0.75→1.1 V_{NHE} potential jumps (top) and 1.2→1.35 V_{NHE} potential jumps (bottom). B) Time courses of potential-induced Co X-ray fluorescence changes for excitation at 7720.8 eV, measured simultaneously with the current densities of panel A. At the chosen X-ray excitation energy, the X-ray fluorescence intensity change reflects predominantly Co oxidation-state changes; a signal decrease corresponds to Co oxidation and a signal increase corresponds to Co reduction (Figure S17, Supporting Information). Traces were normalized to a summed amplitude of unity. Lines show bi-exponential simulations with time constants for the 0.75→1.1 V_{NHE} (1.2→1.35 V_{NHE}) of about 380 ms (250 ms) for the fast phase and about 3.9 s (3.7 s) for the slow phase. The corresponding transients for the reverse jumps from high to low potential are shown in Figure S17, Supporting Information; fit parameters are listed in Table S6, Supporting Information. For further experimental details see Figure S16, Supporting Information.

consequently both phases require charge-compensating ion flow. Here, the fast Co oxidation phase is of special interest because it is, with time constants of below 400 ms it is minimally by one order of magnitude faster than the K^+ release kinetics with its fast-phase time constant of 4–8 s (Figure 5 and Table S6, Supporting Information), precluding transient K^+ release in an initial phase of the cobalt redox transitions. The slow phase may relate to oxidation-state changes coupled to slow structural changes (currently under investigation). Notably, also a respective potential jump into reducing direction reveals cobalt reduction on a millis scale (Figure S17, Supporting Information), further supporting the kinetic mismatch between the K^+ ion exchange and the cobalt redox transitions.

3. Conclusions

(1) What is the structural role of K^+ ions bound within the CoCat material?

Operation in low-concentration potassium phosphate electrolyte (1.6 vs 100 mM KPi) results in a CoCat with low K^+ content (threefold diminished). As previously shown,[32] for electrochemical operation of this low-K^+ CoCat, the potential dependence of the Co oxidation states and coordination environment does not differ from that of the high-K^+ CoCat, indicating a non-essential role of K^+ ions for the atomic structure and electrochemical functionality. This conclusion is supported by similar CoCat structure also after K^+ versus Na^+ exchange. The latter finding is opposed to the effect of phosphate exchange (vs actetate,[13] chloride,[13] or arsenate[60]), which alters both properties. That CoCat-internal K^+ is structurally innocent, is in line with our analysis of the K^+ coordination, which reveals that tight binding to three Co ions to form a cubane motif, as found for Ca^{2+} in the Mn_4Ca-oxo cluster of the biological catalyst of photosystem II[34–37] and also in inorganic OER catalyst materials,[34–37] is not relevant for K^+ in CoCat. Instead, a sizeable fraction of otherwise hydrated K^+ ions likely forms ion pairs with phosphate species, resulting in a K^+ coordination environment similar to that found in concentrated KPi solution. In summary, the properties of K^+ within the CoCat are in agreement with a dissolved ion in the aqueous quasi-electrolyte[8] that fills the space between Co oxide fragment layers without any direct influence on structure, redox chemistry, and catalytic performance of the material.

(2) Do K^+ ions facilitate charge compensation in the redox transitions of the catalyst material?

The volume activity of the CoCat material implies that Co oxidation state changes are associated with charge-compensating ion flows that prevent charge accumulation in the catalyst interior. This means that Co oxidation within the macroscopic catalyst volume needs to be associated with a corresponding quantity of cations (incl. protons) leaving the catalyst volume (or anions entering it); reversed ion flows are expected for Co reduction. Our analysis of the K^+ binding mode suggests loose binding in the hydrated layered oxide material as part of interlayer

quasi-electrolyte. Based on the observed rapid exchangeability of most if not all K^+ ions within the CoCat, charge compensating K^+ flow may appear as a plausible option. However, analysis of the elemental composition of the CoCat material equilibrated at reducing and oxidizing potentials reveals that potential-dependent Co oxidation is associated neither with K^+ depletion nor with phosphate enrichment (see Figure 1).

The temporal sequence of events associated with the potential-induced Co oxidation might involve K^+ release as a fast initial response to an increased electrode potential, followed by Co oxidation associated with deprotonation of Co ligands paralleled by a reverse K^+ uptake. This per se plausible scenario was excluded herein by time-resolved X-ray experiments revealing clearly faster Co oxidation (around 300 ms) than K^+ release (around 5 s).

Here we conclude that K^+ ions do not serve as counter ions in oxidation-state changes of the CoCat material and likely also do not have any other major functional role. Therefore, it is reasonable to assume that also other redox-inert electrolyte cations such as sodium do not serve as charge-compensating ions. (For technical reasons, the same experiments as pursued in the present study cannot be carried out for sodium-containing CoCat, because of the low X-ray energy of the Na K-edge.)

In conclusion, the stoichiometric charge compensation in the Co redox transitions of the volume-active CoCat material is not facilitated by any ions aside from protons. Early electrokinetic investigations have provided evidence that OER involves proton-coupled electron transfer reactions in CoCat, pointing toward coupling of the $Co^{3+/4+}$ oxidation to proton release.[26,31] The coupling to proton release and uptake is in line with the clear pH-dependence[7,8,24] and H/D isotope effect[31] of the midpoint potential of the Co redox transitions.[7,23] At atomic level, the proton release coupled to Co oxidation likely proceeds by deprotonation of Co water species (H_2O, OH^-) coordinated to Co ions, as previously suggested based on structural changes detected by XAS,[7] later supported by the H/D exchange influence on electrokinetic data[31] and operando Raman spectra.[61]

(3) Relevance for other catalyst materials

The structural changes associated with the $Co^{2+/3+}$ and $Co^{3+/4+}$ redox transitions of the CoCat material are comparably moderate; non-stoichiometric mixed-valence Co oxidation states ($Co^{2+}_{0.4}Co^{3+}_{0.6}$ and $Co^{3+}_{0.8}Co^{4+}_{0.2}$, respectively) are encountered at lowest and highest potentials.[7] In other OER catalyst materials, potential-induced redox transitions are coupled to clearly more pronounced structural changes and more complete redox transitions, thus corresponding to a full-fledged phase transition. A prime example is layered Ni-based oxyhydroxides, for which the $Ni^{2+/3+}$ transition is associated with increasing layer spacing, likely involving water as well as K^+ ion insertion.[42] In the latter material the structural and charge-compensating role of K^+ ions may differ from the one in the CoCat and related amorphous materials.

The CoCat is a dynamic material for which redox activity and catalytic activity are not restricted to the bulk-electrolyte exposed surface, but are occurring in the complete bulk volume of the catalyst material (volume activity),[8] even for the ≈700 nm material thickness of the 100 mC cm^{-2} CoCat as used in the present study.[8] On a first glance, this volume activity appears as a very special property. However, by prolonged OER operation several initially crystalline, molecular, and metallic catalyst materials were transformed partially or completely into an amorphous material with similar redox properties of the amorphized regions as observed for the bulk-volume of the CoCat.[43,35,62–74] Therefore we believe that the here reported findings on the K^+ binding mode and likely absence of a charge-compensating role of K^+ ions are of relevance for a larger group of OER-active materials, but possibly not for OER materials where the redox transitions exhibit phase-transition character. For optimization of charge-compensating ion flows in volume-active OER materials, rather than catalyst-internal cations, the (de)protonation reactions and proton mobility may be especially promising targets.

Supporting Information

Supporting Information is available from the Wiley Online Library or from the author.

Acknowledgements

This work was funded by the Deutsche Forschungsgemeinschaft (DFG, German Research Foundation) under Germany's Excellence Strategy—EXC 2008/1–390540038—UniSysCat and the German Federal Ministry of Education and Research (BMBF project "Live-XAS"). S.L. gratefully acknowledges support by the China Scholarship Council (CSC) in form of a doctoral fellowship. S.F. was funded by the Einstein Foundation Berlin (Einstein Cluster EC^2). The authors thank the Helmholtz-Zentrum Berlin (HZB) for beamtime allocation at the KMC-3 synchrotron beamline of the BESSY synchrotron in Berlin-Adlershof and Dr. Ivo Zizak as well as further HZB staff for technical support.

Open access funding enabled and organized by Projekt DEAL.

Conflict of Interest

The authors declare no conflict of interest.

Data Availability Statement

The data that support the findings of this study are available in the supplementary material of this article.

Keywords

cobalt oxyhydroxide, operando spectroscopy, oxygen evolution reaction, electrocatalysis, X-ray absorption spectroscopy

Received: January 10, 2023
Revised: March 23, 2023
Published online: May 19, 2023

[1] J. Li, C. A. Triana, W. Wan, D. P. A. Saseendran, Y. Zhao, S. E. Balaghi, S. Heidari, G. R. Patzke, *Chem. Soc. Rev.* **2021**, *50*, 2444.
[2] W. J. Jiang, T. Tang, Y. Zhang, J. S. Hu, *Acc. Chem. Res.* **2020**, *53*, 1111.
[3] R. Matheu, P. Garrido-Barros, M. Gil-Sepulcre, M. Z. Ertem, X. Sala, C. Gimbert-Suriñach, A. Llobet, *Nat. Rev. Chem.* **2019**, *3*, 331.

[4] B. M. Hunter, H. B. Gray, A. M. Müller, *Chem. Rev.* **2016**, *116*, 14120.
[5] H. Dau, C. Limberg, T. Reier, M. Risch, S. Roggan, P. Strasser, *ChemCatChem* **2010**, *2*, 724.
[6] M. Plevová, J. Hnát, K. Bouzek, *J. Power Sources* **2021**, *507*, 230072.
[7] M. Risch, F. Ringleb, M. Kohlhoff, P. Bogdanoff, P. Chernev, I. Zaharieva, H. Dau, *Energy Environ. Sci.* **2015**, *8*, 661.
[8] K. Klingan, F. Ringleb, I. Zaharieva, J. Heidkamp, P. Chernev, D. Gonzalez-Flores, M. Risch, A. Fischer, H. Dau, *ChemSusChem* **2014**, *7*, 1301.
[9] X. Bo, R. K. Hocking, S. Zhou, Y. Li, X. Chen, J. Zhuang, Y. Du, C. Zhao, *Energy Environ. Sci.* **2020**, *13*, 4225.
[10] B. Wang, K. Zhao, Z. Yu, C. Sun, Z. Wang, N. Feng, L. Mai, Y. Wang, Y. Xia, *Energy Environ. Sci.* **2020**, *13*, 2200.
[11] R. D. L. Smith, C. Pasquini, S. Loos, P. Chernev, K. Klingan, P. Kubella, M. R. Mohammadi, D. Gonzalez-Flores, H. Dau, *Nat. Commun.* **2017**, *8*, 2022.
[12] G.-F. Li, M. Divinagracia, M. F. Labata, J. D. Ocon, P.-Y. A. Chuang, *ACS Appl. Mater. Interfaces* **2019**, *11*, 33748.
[13] M. Risch, K. Klingan, F. Ringleb, P. Chernev, I. Zaharieva, A. Fischer, H. Dau, *ChemSusChem* **2012**, *5*, 542.
[14] A. C. Garcia, T. Touzalin, C. Nieuwland, N. Perini, M. T. M. Koper, *Angew. Chem., Int. Ed.* **2019**, *58*, 12999.
[15] V. B. R. Boppana, S. Yusuf, G. S. Hutchings, F. Jiao, *Adv. Funct. Mater.* **2013**, *23*, 878.
[16] S. Lee, L. Bai, X. Hu, *Angew. Chem., Int. Ed.* **2020**, *59*, 8072.
[17] Y. Duan, N. Dubouis, J. Huang, D. A. Dalla Corte, V. Pimenta, Z. J. Xu, A. Grimaud, *ACS Catal.* **2020**, *10*, 4160.
[18] J. Huang, M. Li, M. J. Eslamibidgoli, M. Eikerling, A. Groß, *JACS Au* **2021**, *1*, 1752.
[19] M. Fu, G. Ning, J. Liu, Q. Zhang, Y. Sun, X. Fan, H. Wang, H. Lu, Y. Zhang, H. Wang, *Int. J. Hydrogen Energy* **2021**, *46*, 15124.
[20] V. Kotha, I. Karajagi, P. C. Ghosh, L. S. Panchakarla, *ACS Appl. Mater. Interfaces* **2022**, *5*, 7297.
[21] Y. Zhang, M. Xu, X. Xu, X. Li, G. Zhu, G. Jia, B. Yang, R. Yin, P. Gao, W. Ye, *Nanoscale* **2023**, *15*, 204.
[22] M. W. Kanan, D. G. Nocera, *Science* **2008**, *321*, 1072.
[23] M. W. Kanan, J. Yano, Y. Surendranath, M. Dinca, V. K. Yachandra, D. G. Nocera, *J. Am. Chem. Soc.* **2010**, *132*, 13692.
[24] Y. Surendranath, M. W. Kanan, D. G. Nocera, *J. Am. Chem. Soc.* **2010**, *132*, 16501.
[25] W. H. Casey, J. G. Mcalpin, Y. Surendranath, M. Dinca, T. A. Stich, S. A. Stoian, D. G. Nocera, R. D. Britt, *J. Am. Chem. Soc.* **2010**, *132*, 6882.
[26] M. D. Symes, Y. Surendranath, D. A. Lutterman, D. G. Nocera, *J. Am. Chem. Soc.* **2011**, *133*, 5174.
[27] A. J. Esswein, Y. Surendranath, S. Y. Reece, D. G. Nocera, *Energy Environ. Sci.* **2011**, *4*, 499.
[28] M. Risch, V. Khare, I. Zaharieva, L. Gerencser, P. Chernev, H. Dau, *J. Am. Chem. Soc.* **2009**, *131*, 6936.
[29] M. Risch, K. Klingan, I. Zaharieva, H. Dau, in *Molecular Water Oxidation Catalysis* (Ed: A. Llobet), Wiley, New York **2014**, p. 163.
[30] H. Dau, C. Pasquini, *Inorganics* **2019**, *7*, 20.
[31] C. Pasquini, I. Zaharieva, D. Gonzalez-Flores, P. Chernev, M. R. Mohammadi, L. Guidoni, R. D. L. Smith, H. Dau, *J. Am. Chem. Soc.* **2019**, *141*, 2938.
[32] S. Liu, I. Zaharieva, L. D'amario, S. Mebs, P. Kubella, F. Yang, P. Beyer, M. Haumann, H. Dau, *Adv. Energy Mater.* **2022**, *12*, 2202914.
[33] C. Pasquini, S. Liu, P. Chernev, D. Gonzalez-Flores, M. R. Mohammadi, P. Kubella, S. Jiang, S. Loos, K. Klingan, V. Sikolenko, S. Mebs, M. Haumann, P. Beyer, L. D'amario, R. D. L. Smith, I. Zaharieva, H. Dau, *Anal. Bioanal. Chem.* **2021**, *413*, 5395.
[34] D. González-Flores, I. Zaharieva, J. Heidkamp, P. Chernev, E. Martinez-Moreno, C. Pasquini, M. R. Mohammadi, K. Klingan, U. Gernet, A. Fischer, H. Dau, *ChemSusChem* **2016**, *9*, 379.
[35] I. Zaharieva, M. M. Najafpour, M. Wiechen, M. Haumann, P. Kurz, H. Dau, *Energy Environ. Sci.* **2011**, *4*, 2400.
[36] E. Baktash, I. Zaharieva, M. Schröder, C. Goebel, H. Dau, A. Thomas, *Dalton Trans.* **2013**, *42*, 16920.
[37] Y. Mousazade, M. R. Mohammadi, R. Bagheri, R. Bikas, P. Chernev, Z. Song, T. Lis, M. Siczek, N. Noshiranzadeh, S. Mebs, H. Dau, I. Zaharieva, M. M. Najafpour, *Dalton Trans.* **2020**, *49*, 5597.
[38] H. Dau, A. Grundmeier, P. Loja, M. Haumann, *Philos. Trans. R. Soc., B* **2008**, *363*, 1237.
[39] K. N. Ferreira, T. M. Iverson, K. Maghlaoui, J. Barber, S. Iwata, *Science* **2004**, *303*, 1831.
[40] Y. Umena, K. Kawakami, J.-R. Shen, N. Kamiya, *Nature* **2011**, *473*, 55.
[41] C. Yang, G. Rousse, K. Louise Svane, P. E. Pearce, A. M. Abakumov, M. Deschamps, G. Cibin, A. V. Chadwick, D. A. D. Corte, H. A. Hansen, T. Vegge, J.-M. Tarascon, A. Grimaud, *Nat. Commun.* **2020**, *11*, 1378.
[42] F. Dionigi, Z. Zeng, I. Sinev, T. Merzdorf, S. Deshpande, M. B. Lopez, S. Kunze, I. Zegkinoglou, H. Sarodnik, D. Fan, A. Bergmann, J. Drnec, J. F. D. Araujo, M. Gliech, D. Teschner, J. Zhu, W.-X. Li, J. Greeley, B. R. Cuenya, P. Strasser, *Nat. Commun.* **2020**, *11*, 2522.
[43] D. Gonzalez-Flores, I. Sanchez, I. Zaharieva, K. Klingan, J. Heidkamp, P. Chernev, P. W. Menezes, M. Driess, H. Dau, M. L. Montero, *Angew. Chem., Int. Ed.* **2015**, *54*, 2472.
[44] M. Risch, F. Ringleb, V. Khare, P. Chernev, I. Zaharieva, H. Dau, *J. Phys.: Conf. Ser.* **2009**, *190*, 012167.
[45] A. E. Thorarinsdottir, D. G. Nocera, *Chem Catal.* **2021**, *1*, 32.
[46] M. Wiechen, I. Zaharieva, H. Dau, P. Kurz, *Chem. Sci.* **2012**, *3*, 2330.
[47] S. Boyd, K. Ganeshan, W. Y. Tsai, T. Wu, S. Saeed, D. E. Jiang, N. Balke, A. C. T. Van Duin, V. Augustyn, *Nat. Mater.* **2021**, *20*, 1689.
[48] P. H. Benhangi, A. Alfantazi, E. Gyenge, *Electrochim. Acta* **2014**, *123*, 42.
[49] B. M. Hunter, W. Hieringer, J. R. Winkler, H. B. Gray, A. M. Muller, *Energy Environ. Sci.* **2016**, *9*, 1734.
[50] S. Dresp, F. Dionigi, M. Klingenhof, T. Merzdorf, H. Schmies, J. Drnec, A. Poulain, P. Strasser, *ACS Catal.* **2021**, *11*, 6800.
[51] A.-C. Gaillot, D. Flot, V. A. Drits, A. Manceau, M. Burghammer, B. Lanson, *Chem. Mater.* **2003**, *15*, 4666.
[52] V. Vao-Soongnern, C. Pipatpanukul, S. Horpibulsuk, *J. Mater. Sci.* **2015**, *50*, 7126.
[53] P. W. Du, O. Kokhan, K. W. Chapman, P. J. Chupas, D. M. Tiede, *J. Am. Chem. Soc.* **2012**, *134*, 11096.
[54] G. Kwon, H. Jang, J.-S. Lee, A. Mane, D. J. Mandia, S. R. Soltau, L. M. Utschig, A. B. F. Martinson, D. M. Tiede, H. Kim, J. Kim, *J. Am. Chem. Soc.* **2018**, *140*, 10710.
[55] C. N. Brodsky, D. K. Bediako, C. Shi, T. P. Keane, C. Costentin, S. J. L. Billinge, D. G. Nocera, *ACS Appl. Mater. Interfaces* **2019**, *2*, 3.
[56] H. Dau, P. Liebisch, M. Haumann, *Anal. Bioanal. Chem.* **2003**, *376*, 562.
[57] V. A. Glezakou, Y. S. Chen, J. L. Fulton, G. K. Schenter, L. X. Dang, *Theor. Chem. Acc.* **2006**, *115*, 86.
[58] C. N. Rowley, B. T. Roux, *J. Chem. Theory Comput.* **2012**, *8*, 3526.
[59] D. Zhuang, M. Riera, R. Zhou, A. Deary, F. Paesani, *J. Phys. Chem. B* **2022**, *126*, 9349.
[60] J. Villalobos, D. Gonzalez-Flores, K. Klingan, P. Chernev, P. Kubella, R. Urcuyo, C. Pasquini, M. R. Mohammadi, R. D. L. Smith, M. L. Montero, H. Dau, *Phys. Chem. Chem. Phys.* **2019**, *21*, 12485.
[61] C. Pasquini, L. D'amario, I. Zaharieva, H. Dau, *J. Chem. Phys.* **2020**, *152*, 194202.
[62] M. Risch, K. Klingan, J. Heidkamp, D. Ehrenberg, P. Chernev, I. Zaharieva, H. Dau, *Chem. Commun.* **2011**, *47*, 11912.
[63] A. Bergmann, E. Martinez-Moreno, D. Teschner, P. Chernev, M. Gliech, J. F. De Araujo, T. Reier, H. Dau, P. Strasser, *Nat. Commun.* **2015**, *6*, 8625.
[64] P. W. Menezes, C. Panda, C. Walter, M. Schwarze, M. Driess, *Adv. Funct. Mater.* **2019**, *29*, 1808632.

[65] J. N. Hausmann, S. Mebs, H. Dau, M. Driess, P. W. Menezes, *Adv. Mater.* **2022**, *34*, 2207494.
[66] J. Villalobos, D. González-Flores, R. Urcuyo, M. L. Montero, G. Schuck, P. Beyer, M. Risch, *Adv. Energy Mater.* **2021**, *11*, 2101737.
[67] K. J. May, C. E. Carlton, K. A. Stoerzinger, M. Risch, J. Suntivich, Y.-L. Lee, A. Grimaud, Y. Shao-Horn, *J. Phys. Chem. Lett.* **2012**, *3*, 3264.
[68] M. Risch, A. Grimaud, K. J. May, K. A. Stoerzinger, T. J. Chen, A. N. Mansour, Y. Shao-Horn, *J. Phys. Chem. C* **2013**, *117*, 8628.
[69] S. W. Lee, C. Carlton, M. Risch, Y. Surendranath, S. Chen, S. Furutsuki, A. Yamada, D. G. Nocera, Y. Shao-Horn, *J. Am. Chem. Soc.* **2012**, *134*, 16959.
[70] J. D. Blakemore, M. W. Mara, M. N. Kushner-Lenhoff, N. D. Schley, S. J. Konezny, I. Rivalta, C. F. A. Negre, R. C. Snoeberger, O. Kokhan, J. Huang, A. Stickrath, L. A. Tran, M. L. Parr, L. X. Chen, D. M. Tiede, V. S. Batista, R. H. Crabtree, G. W. Brudvig, *Inorg. Chem.* **2013**, *52*, 1860.
[71] E. R. Young, D. G. Nocera, V. Bulović, *Energy Environ. Sci.* **2010**, *3*, 1726.
[72] S. Loos, I. Zaharieva, P. Chernev, A. Lißner, H. Dau, *ChemSusChem* **2019**, *12*, 1966.
[73] S. Yan, K. P. Abhilash, L. Tang, M. Yang, Y. Ma, Q. Xia, Q. Guo, H. Xia, *Small* **2019**, *15*, 1804371.
[74] Y. Zhou, H. J. Fan, *ACS Mater. Lett.* **2021**, *3*, 136.